Contributions to Geophysics and Geodesy Vol. 55/4, 2025 (503–538)

Unveiling crustal intrusions and fault systems of southwestern Sokoto Basin through enhanced gravity analysis

Adamu ABUBAKAR[1,*], Othniel Kamfani LIKKASON[2], Abdulganiyu YUNUSA[3]

[1] Department of Applied Geophysics, Federal University Birnin Kebbi, P.M.B 1157, Kebbi State, Nigeria;
e-mail: adamu.abubakar35@fubk.edu.ng

[2] Department of Physics, Abubakar Tafawa Balewa University Bauchi, P.M.B 1051, Bauchi State, Nigeria;
e-mail: likkason@yahoo.com

[3] Department of Geology, Federal University Birnin Kebbi, P.M.B 1157, Kebbi State, Nigeria;
e-mail: yunusa.abdulganiyu@fubk.edu.ng

Abstract: The Sokoto Basin, a frontier basin area in northwestern Nigeria, has garnered significant attention due to its favourable prospects for oil and gas exploration. This study utilises potential field gravity data to investigate the depth architecture of the southwestern Sokoto Basin and provide insights into the emplacement mechanisms of its anomalous geological features. The Bouguer gravity anomaly reveals a regional gravity field dipping at approximately 10° northeasterly, with a gradient of 0.38 mGal/km. Residual Bouguer anomaly analysis identifies a prominent positive anomaly in the southern region and negative anomalies ranging from −74.88 mGal to −27.38 mGal. Integration of enhancement filters, forward modelling, and spectral analysis reveals that source depths increase towards the south. Gravity modelling indicates intrusions in the upper crust at depths of 10 to 20 km and 5 to 10 km. A 3D model assembled from the findings illustrates the basin's subsurface structure, supporting earlier works. The results suggest that Eocene sediments and Quaternary faults/fractures play critical roles in the area's hydrocarbon system. Ultimately, the quantitative analysis of the gravity maps reveals the presence of diverse structural features and their constituent components within the study area. Notably, the primary tectonic deformations exhibit trends oriented NW–SE, NE–SW, and E–W. This study significantly enhances our understanding of the subsurface architecture of the southwestern Sokoto Basin, offering crucial insights that will inform and optimise future hydrocarbon exploration initiatives.

Key words: gravity data, enhancement utilisation, depth estimation, geological structures, modelling, Sokoto basin

*corresponding author, e-mail: adamu.abubakar35@fubk.edu.ng

doi: 10.31577/congeo.2025.55.4.5

1. Introduction

With the upbeat of petroleum exploration activities in Nigeria's inland basins attention is focused on the analyses of structural patterns in the area. The Sokoto Basin, forming a significant part of the Iullemmeden Basin, has drawn to attention of workers in the prospect for petroleum system and set of this sub-basin. Potential field methods, particularly gravity and magnetic surveys, have proven instrumental in delineating subsurface features and evaluating hydrocarbon systems (*Copper, 1997; Dobrin, 1976; Hinze et al., 2013; Reid and Thurston, 2014*). These methods rely on contrasts in physical properties (density and magnetisation variations in crustal rocks) to infer geologic structures relevant as hosts to hydrocarbon accumulation, migration pathways and other mineralisation.

Despite this progress, several knowledge gaps persist. The role of deep crustal intrusions in hydrocarbon migration within the basin remains unquantified. Additionally, the spatial configuration and effectiveness of fault-controlled hydrocarbon traps are not well understood. Integrated geophysical studies, combining gravity, magnetic, and seismic data, are notably absent from most of these inland basins including the Sokoto basin. Intrusive bodies associated with hydrocarbon source rocks have not been comprehensively characterised, and the links between basement configurations and petroleum system development remain uncertain.

Furthermore, recent advancements in gravity data processing, such as enhanced balanced total horizontal gradient (EBTHG) and directional filtering offer improved edge detection capabilities (*Fairhead, 1986; Pham et al., 2024; Pham, 2023; Mohamed and Al Deep, 2021*) that can improve and expose exploration targets in a more robust way. The comparative performance of such filters has not been tested over the regions covering the Nigerian inland basins as there is no documentation as such. The basin-wide variability in source depth and its geological implications also require further refinement using enhanced digital tools.

To address these gaps, this study employs both qualitative and quantitative gravity interpretation techniques, including enhanced balanced total horizontal gradient (EBTHD), directional filtering, spectral analysis, Werner depth solutions, and 2D forward modelling of the gravity data (*Adamu et al., 2021; Abraham et al., 2025; Chen et al., 2016; Chen, 2019;*

Nwankwo, 2015; Ku and Sharp, 1983; Likkason et al., 2013; Likkason, 2011; Reid et al., 1990; Reid and Thurston, 2014; Salem et al., 2007, 2011). The tools are applied to the Bouguer gravity anomaly data over this part of the Sokoto basin, primarily to delineate subsurface structures and assess their potentials as hosts for hydrocarbon and mineral accumulations. The findings are significant and would throw more light on the basin's tectonic framework and recommendations that would assist future exploration efforts over this and similar basins.

2. Location and geological context of the area

A significant sub-Saharan inland sedimentary basin in West Africa, the Iullemmeden Basin includes the Sokoto Basin and extends over western Niger, Algeria, Mali, and Nigeria (Figs. 1 and 2). This study focuses on the southwestern part of the Sokoto Basin, situated between 11° 00′ N and 13° 00′ N and longitudes 3° 30′ E and 5° 30′ E. The study area covers approximately 37,600 km^2 (Fig. 2, Table 1) and has an elevation range of 200 to 400 m above sea level.

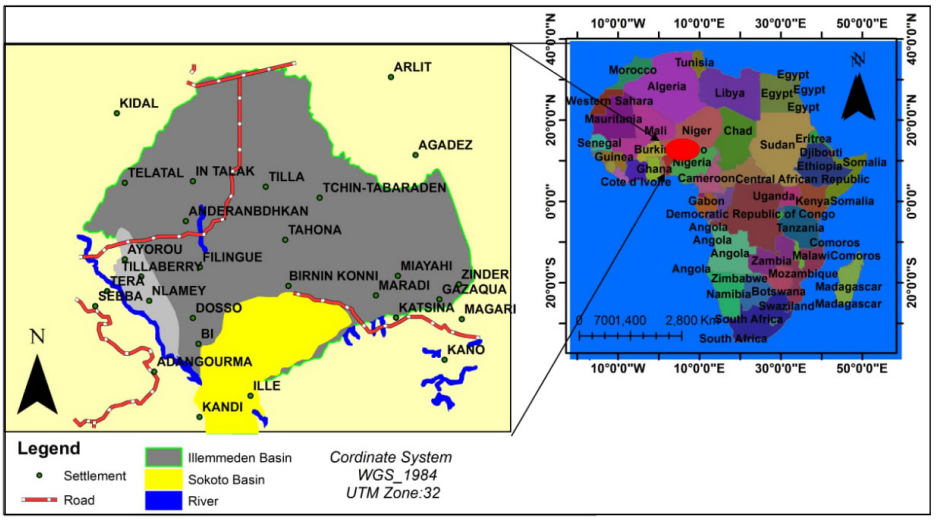

Fig. 1. A global tectonic map of the rifted basins in western, central, and eastern Africa that depicts the connection between the "Sokoto basin" and the other basins where commercially successful oil and gas discoveries have been made.

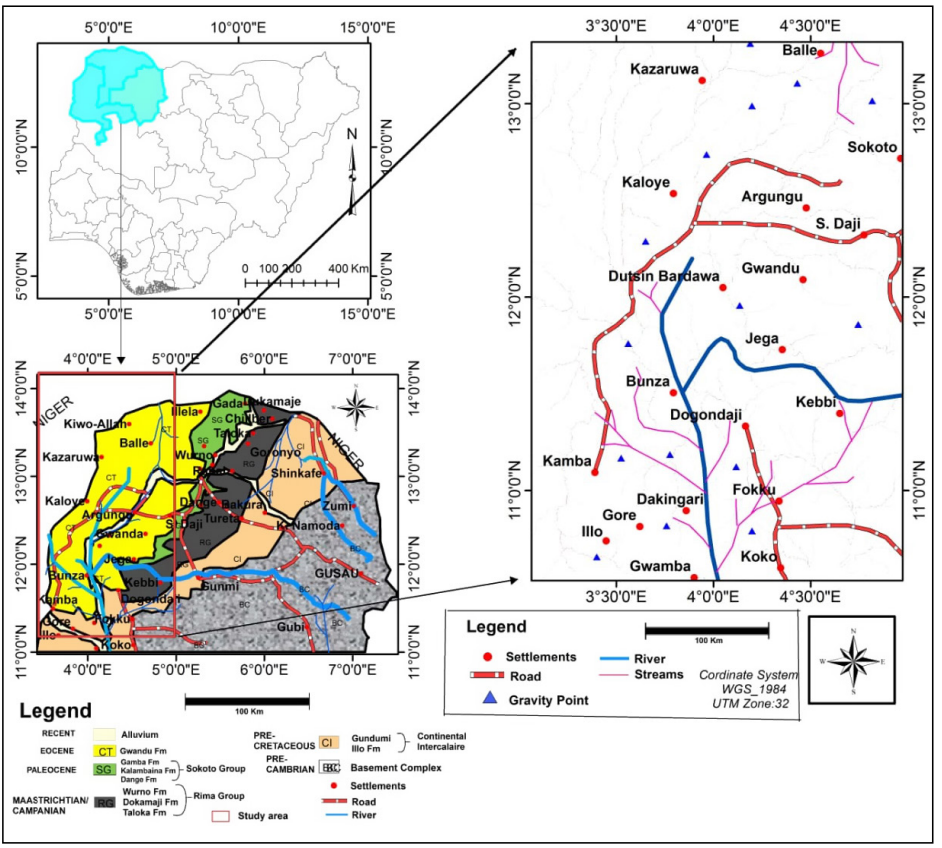

Fig. 2. Location map of Sokoto Basin, its general geology and Study Area with gravity distribution points (*Kogbe, 1979*).

Geologically, the Sokoto Basin is part of the West African Sub-Saharan Sudan belt, characterised by semi-arid region with Savanna-type flora. The basin's tectonic evolution is closely linked to the opening of the Atlantic Ocean and the break-up of the Supercontinent Gondwana (*Kogbe, 1979; Obaje et al., 2013*). The Sokoto Basin underwent rifting and extension during the Late Proterozoic to Early Paleozoic (c. 600 – 400 Ma), followed by thermal subsidence in the Late Paleozoic to Early Mesozoic (c. 300 – 200 Ma) (*Kogbe, 1979*). The opening of the Atlantic Ocean during the Early Cretaceous (c. 130 – 100 Ma) led to another phase of rifting and faulting (*Obaje, 2009; Kogbe, 1979; Kogbe, 1981*).

Table 1. Lithostratigraphic successions of Sokoto Basin sub area after *Kogbe (1979)*.

AGE	FORMATION	DESCRIPTION	GROUP	ENVIRONMENT
(a) EOCENE–MIOCENE	GWANDU	Massive clays with red mottling, intercalated sandstone, and ironstone.	CONTINENTAL TERMINALE	Continental
(b) PALEOCENE	GAMBA	Fossil-rich, grey layered shale.	SOKOTO GROUP	Marine
	KALAMBAINA Calcareous Group	Shale with a wealth of fossils and white clayey limestones. Echinoids, Bivalves, Mollusks, Forams, and Ostracods.		
	DANGE Clay-shale Group	Bluish-grey shale limestone that is slightly indurated, with thin layers of yellowish-brown limestone interbedded with irregular phosphatic nodules and bands of fibrous gypsum.		
(c) MAASTRICHTIAN Upper Senonian	WURNO Upper Sandstones and Mudstones	Iron sulfide-containing carbonaceous mudstone, thin intercalated mudstone, and pale, friable, fine-grained sandstone and siltstone.	RIMA GROUP	Continental
	DUKAMAJE Mosasaurus shale	The bone bed of gypsiferous shale, limestone, and mudstone shale is a great marker horizon. It has a significant fossiliferous content.		Marine
	TALOKA Lower Sandstones and Mudstones	Carbonaceous mudstone or shale with ferruginous and gypsum particles, as well as friable white siltstone and sandstone with fine-grained, thin intercalated mudstone.		Continental
(d) PRE-MAASTRICHTIAN	GUNDUMI	Sand, gravel, pisolithic and nodular clays, and basal conglomerates, fossiliferous in poor quality.	CONTINENTAL INTERCALAIRE	Lacustrine and Fluvial
	ILLO	The Upper Grits Nodular and Pisolithic Clays Reduced Grits		
PRECAMBRIAN	BASEMENT COMPLEX			

The study area comprises rugged and resistant sedimentary deposits, forming gently undulating plains and flat-topped hills that cut across the entire formations in the Sokoto Basin. A moderate undulating plain with varying elevation makes up a major part of the Sokoto sedimentary basin, northwestern Nigeria. The terrain is dominated by gently to moderately undulating plains, interrupted by flat-topped, steep-sided hills such as the prominent "Dange Scarp" (*Kogbe, 1981*) although extensive erosion has obscured its original features.

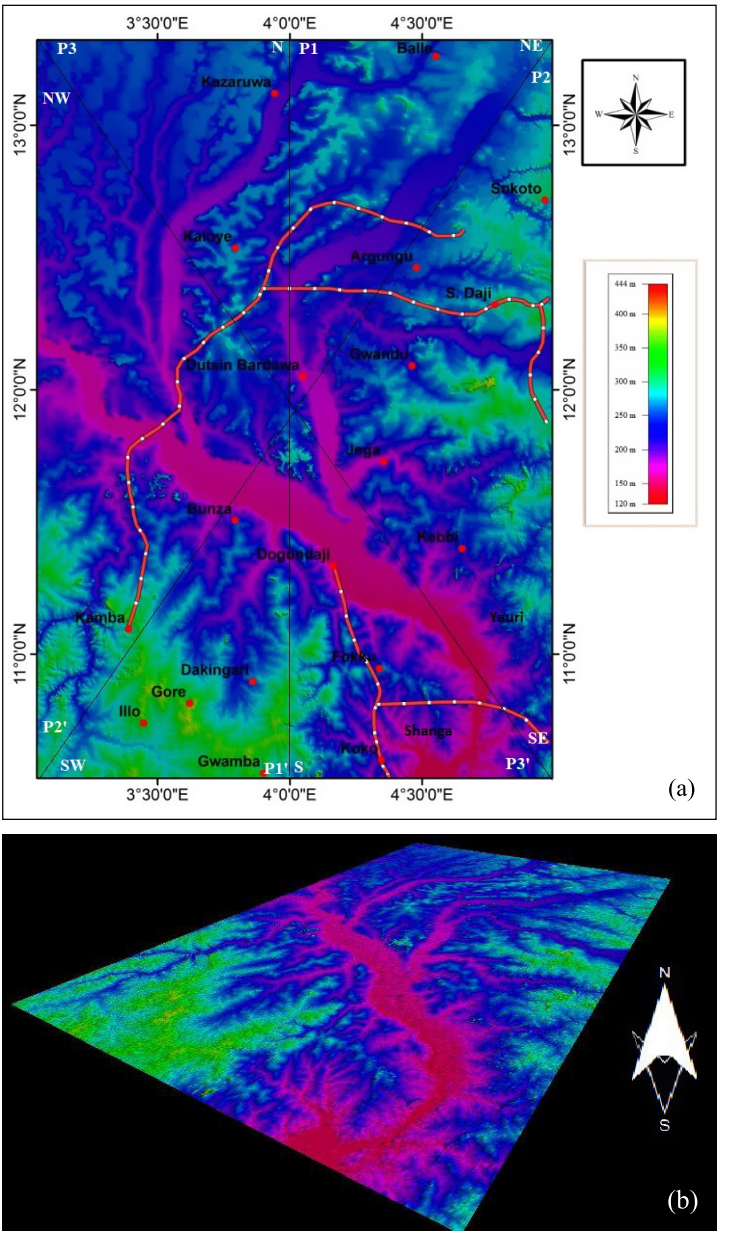

Fig. 3. (a) The study area's topographic map created using ASTER GDEM (ver. 3); (b) ASTER-based three-dimensional topographic map of the area.

The topography and surface elevations of the rock units in the study area were used to create the 30 metre accurate ASTER Global Digital Elevation Model (Fig. 3a). The correlation between altitudes and lithological units provides valuable information for pinpointing rock units and determining the crustal framework over the Sokoto Basin. For instance, the highest topographies reflect the late-to-post tectonic Gundumi/Illo formations, which range in altitude from 300 to 550 m.

The study area's geomorphological characteristics, including terrain, elevation, and environmental relief, provide insights into potential mineralisation controls, and the indices of the subsurface vertical and horizontal borders from a depth of 30 m are shown in Fig. 3b.

3. Methodology

3.1. Gravity data acquisition and processing

To investigate the upper lithospheric structures beneath the southwestern part of the Sokoto Basin and its surroundings, gravity measurements were collected, analysed, and processed. The gravity method detects variations in the horizontal density distribution of subsurface materials (*Cooper, 1997; Dobrin, 1976; Telford et al., 1990*). This technique has been widely applied in developing conceptual exploration models, identifying prospective hydrocarbon-bearing zones, and conducting regional crustal characterisation (*Hinze et al., 2013; Salem et al., 2011; Treitel et al., 1967*). A total of 1,095 gravity stations were established across the study area, with an inter-station spacing ranging from 0.5 to 1 km (some representative location shown in Fig. 2). The survey traverses were oriented northwest-southeast and tied to three primary absolute gravity stations within the Sokoto Basin:

- Birnin Kebbi (90010, 978171.260 mGal),
- Daki-Takwas (90011, 978135.860 mGal), and
- Sokoto (90012, 978184.039 mGal).

Gravity measurements were acquired using a Lacoste and Romberg gravimeter (Model CG-725).

Standard corrections were effected for instrumental drift and Earth tides, elevation and simple Bouguer slab and even though the study area has a near-plain topography the terrain corrections were ignored in the calcula-

tions. Prior to the field work, the instrument drift/earth tides were observed over a period of 6 days at the Geophysical Laboratory of Federal University Birnin Kebbi, Nigeria. The mean drift rate was +0.12 mGal per 24 hours with a maximum of +0.12 mGal in 6 hours. Because of this low value it was felt that it would be justifiable to take few hours to elapse between drift checks. From drift curves (not shown), the drift was linear between consecutive base-station readings. The majority of ties between two bases A and B were made by an outward and return journey only, i.e. sequence of A–B–A. During the outward A–B journey, intermediate stations were established at approximately two-km intervals. Where it appeared important to determine a relatively steep gravity gradient more precisely, additional stations were put in at 1-km intervals or less on the return journey. Station positions were fixed by use of global positioning system (GPS). Latitude corrections followed the IGR-1967: the 1967 International Gravity Formula (*Hinze et al., 2013; Salem et al., 2011*). Bouguer anomalies were computed using a reduction density of 2.60 gcm^{-3}, representing the average density of exposed lithologies in the study area. Terrain corrections were calculated in Geosoft Montage$^{\mathrm{TM}}$ using methods from *Jacobsen (1987)* and *Kebede et al. (2020)*, yielding the terrain corrected Bouguer gravity anomaly data. The latitude correction was handled by the use of IGR-67 expressed as:

$$g_\theta = 978171.260\,(1 + 0.005278895\sin^2\theta + 0.000023462\sin^4\theta)\,,$$

where g_θ is the predicted value of gravity in mGal and θ is the latitude. The regional gravity field was removed by applying a high-pass filter with a cut-off wavelength of 20 km. This process isolated residual anomalies representing short-wavelength, shallow sources—by subtracting both the 5 km upward-continued field and a first-order trend surface from the Bouguer gravity anomaly data. The resulting residual anomaly maps were compared with directionally filtered gravity anomaly maps to evaluate the extent of resolution of the shallow subsurface features.

Three gravity profiles, trending NE–SW, NW–SE, and N–S were quantitatively analysed using the 2.5-D (GM-SYS) modelling program to characterise the subsurface structures of the study area. The models were constrained by mapped surface lithologies, with density parameters derived from direct bedrock measurements, ensuring geologically consistent and plausible interpretations.

Data analyses included the generating the complete Bouguer anomaly (CBA), and regional-residual separation of the CBA. Enhancement filters from Geosoft Oasis Montaj software were applied. Advanced geophysical techniques, such as power spectrum analysis, Werner deconvolution, and forward modelling (2D and 3D) were used to analyse and model the data, focusing on estimating depths and dips of the geological formations.

3.1.1. Regional-residual separation technique

Potential fields are projected from one datum to another using the mathematical technique known as upward continuation (*Agarwal and Sivaji, 1992; Copper, 1997*). By using this technique, an anomaly is produced that gives the impression that the data were collected at a higher level. If a potential field is carried upward to a height of z, anomaly sources can be found at and below a depth of $z/2$ (*Agarwal and Sivaji, 1992*).

3.2. Digital filtering tools apply for data processing in the study area

Regional and residual components can be distinguished using a variety of methods. The following computer-based Fourier Transform techniques were used in this study:

3.2.1. Enhance balanced total horizontal gradient (EBTHG)

Shallow basement formations and mineral targets are mapped using the enhanced balanced total horizontal gradient (EBTHG) filter (*Copper, 1997; Ai et al., 2023; Hinze et al., 2013; Pham, 2023; Pham and Prasad, 2023; Salem et al., 2007; 2011*). With amplitudes limited between $+\pi/2$ and $-\pi/2$, this filter uses the absolute value of the EBTHG (*Hinze et al., 2013; Salem et al., 2007*). The edges of model structures are where the tilt derivative's zero crossing occurs.

3.2.2. Directional filtering technique

Images moving in a particular direction can have their edges enhanced or attenuated by directional filtering (*Treitel et al., 1967; Bamberger and Smith, 1992; Kowalik and Glenn, 1987; Maithya and Fujimitsu, 2018*). This method is applied to image processing and geophysical research to improve

linear characteristics (*Bamberger and Smith, 1992; Naidu and Matthew, 1998; Naidu, 1968; Thorarinsson et al., 1988*). This study used the filter design process described by *Hu and Rabiner (1972)*, using a filter wedged at 40° and 25° transition zones. The band-pass used in directional filtering is made up of a wedge pointed in a particular direction and plotted against the spatial frequencies u and v (radian/km). The solution is zero outside of the wedge (Fig. 4). The ripples in the pass-band and stop-band are minimised in order to find the filter response in the transition zone (Fig. 4). Features are improved when they are parallel to the pie-slice filter (*Kowalik and Glenn, 1987*).

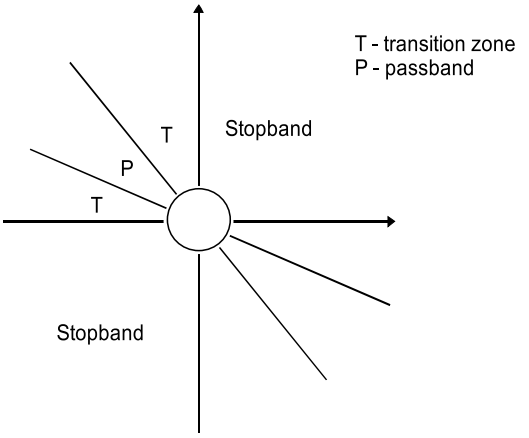

Fig. 4. Directional filter, the pass-band is flanked by transition bands there is circular stop-band over zero frequency; the main aim is to suppress the usually strong power present in the low frequency region.

3.2.3. Spectral analysis of gravity data

The FFT provides the foundation for spectrum analysis of gravity data. Radial averaging is used to construct the energy spectrum using the Geosoft Oasis Montaj MAGMAP algorithm. The Fourier wavenumber domain is used to convert grid data from the space domain (*Spector and Grant, 1970; Fedi and Mastro, 2018; Mishra and Naidu, 1974*).

3.2.4. Werner depth technique of gravity data

To determine the depth of gravity sources, the Werner de-convolution approach is employed (*Hartman et al., 1971; Ku and Sharp, 1983; Werner*

1953; Tarlowski et al., 1996). The 2D Werner de-convolution mathematical model is provided by:

$$F(x) = \frac{Ah + B\,(x - x_0)}{(x - x_0)^2 + h^2}\,, \tag{1}$$

where, x is the distance from some origin along a line perpendicular to the strike of the thin sheet; $F(x)$ is the total field at x; h is the thickness of the thin sheet; and x_0 is the location of the top, projected vertically to intersect the line. The constants A and B relate to the structural gravity characteristics, thickness, and orientation of the thin sheet with respect to the Earth's gravity field.

3.3. Forward modelling of gravity data

The process of forward modelling gravity data entails using potential field measurements to determine the dimensions, form, and physical properties of the field anomaly's source (*Telford et al., 1990*). Iterative quantitative modelling is used to compare the anomaly generated by the computer-aided model with the observed residual anomaly (*Menke, 1989; Talwani et al., 1959*).

4. Results and discussion

4.1. Qualitative interpretation of gravity data

Interpreting gravity data depends critically on the availability of geological data and the precision of gravity surveys. There is enough information about the Sokoto Basin and its environs from earlier geological research (*Kogbe, 1979; Kogbe, 1981; Turner, 1983; Obaje, 2009; Obaje et al., 2013; Ali et al., 2016*). The interpretation of geophysical data is made easier by this knowledge. The complete Bouguer gravity anomaly map of the SW Sokoto Basin reveals three major gravity zones, each with distinct signatures and structural implications: (i) southern zone (high gravity value: −27.38 to −39.29 mGal). These are characterised by NE–SW trending gravity highs, and correspond to basement uplifts or intrusive dyke systems. These features are interpreted as fault-controlled structural highs, likely formed by reactivation of Pan-African basement fabrics during initial rifting phases in the Late Jurassic to Early Cretaceous times. The presence of these

anomalies suggests that the southern zone is underlain by denser lithologies, possibly high-density igneous intrusions or some uplifted fault blocks, (ii) Intermediate zone (intermediate gravity value: −41.47 to −54.02 mGal). This zone exhibits NW–SE trending gravity patterns, indicative of fault-bounded depocentres or tilted crustal blocks formed by oblique extensional tectonics. Residual gravity analysis shows lateral offsets of 10–12 km, particularly along the boundaries of the Sokoto Group and Rima Group units. These offsets, supported by EBTHG and directional filtering maps, are interpreted as basin-scale normal faults that segment the crust and control stratigraphic architecture, (iii) Northern zone (low gravity value: −55.26 to −74.88 mGal). The northern most part of the study area is dominated by pronounced gravity lows with N–S to NW–SE alignment. These anomalies suggest the presence of thick sedimentary accumulation within a structurally down-faulted trough. The continuation of gravity lows at higher altitudes (5–10 km upward continuation) further supports a deep-rooted sedimentary basin or a post-rift sag. The alignment of these features with known seepage zones and continental intercalair (CI) units indicates some bearing with hydrocarbon accumulation and migration.

4.1.1. Topographic, free-air, and complete Bouguer anomaly maps

The terrain of the Sokoto Basin and its environs is unevenly undulating (Fig. 5a). The Gwandu formation's rift flow is at a lower height than the southern and eastern rift borders, which are the highest elevation locations. There is a strong association between the elevation map (Fig. 5a) and the free air anomaly map (Fig. 5b). High-elevation regions, such the Gulma (escarpment features), exhibit negative free air anomalies. Significantly negative free air anomalies, up to −55.84 mGal, are present on the rift floor.

Elevation and spatial variation in the Bouguer anomaly are inversely correlated, as shown by the complete Bouguer anomaly (Fig. 5c). Lower to upper crust density heterogeneities are responsible for the observed gravity anomaly map.

There are gravity highs on the Iullemmeden Basin floor, which follows the Sokoto Basin's northern limit. Whereas gravity low point to less dense subterranean masses, these highs point to denser subsurface masses. Minor high-gravity patches can be found in the northernmost pre-Maastrichtian strata. There is a high gravity region that is heading northeasterly in the

southern part of the research area. (*Hinze et al., 2013; Telford et al., 1990*) These gravity highs may be due to dykes, which are high-density minerals that penetrate from the mantle. Gravity highs and lows are depicted on the map toward the northeast. Denser components inside the Earth's crust may be presumed to function as thermal sources in regions with large gravity anomalies.

4.1.2. Separation of regional-residual gravity field

Isolating relative gravity anomalies or anomalies of significance is crucial when evaluating Bouguer gravity anomalies (*Jacobsen, 1987; Mickus et al.,*

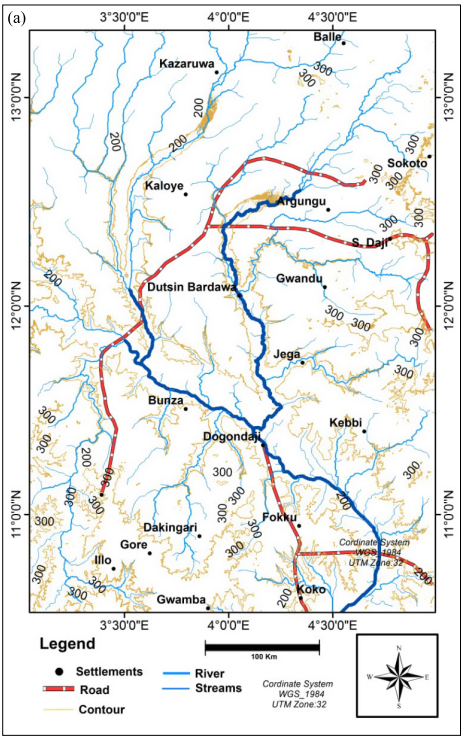

Fig. 5. Southwestern Sokoto Basin geology and geophysical characteristics (a) elevation map displaying the region's topography (b) free air anomaly map of the region (c) map displaying the entire Bouguer anomaly map for the research area. The following labels are applied to important geological features and structures on the maps: CT stands for Continental Terminal Gwandu formation, and SEP for Southeast Plateau. SG stands for Sokoto group Paleocene sediments, RG for Rima group Maastrichtian.

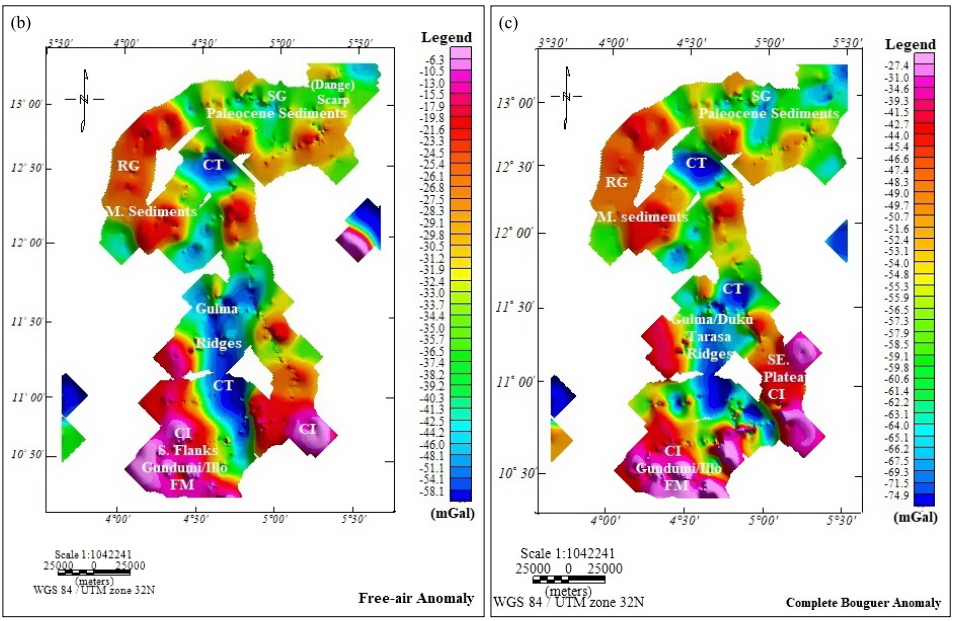

Fig. 5. Continued from the previous page.

2007; Mekkawi et al., 2021; Mekkawi, 2012; Moussa et al., 2020). Regional and residual gravity anomalies make up the observed Bouguer gravity anomaly field. Regional and residual separation techniques were applied to the gravity dataset in order to ascertain the extent of the regional background. By subtracting the regional influence (Fig. 6) from the full Bouguer gravity anomaly (Fig. 5c), the residual gravity anomaly was calculated.

4.1.3. Regional gravity anomaly from upward continuation

Various techniques can be used to characterise the causative bodies of gravity anomalies, depending on the goals. Here, the entire crust underlying the southwestern Sokoto Basin is investigated by looking at the regional anomaly. The complete Bouguer anomaly map (Fig. 5c) was extended upward to form the regional gravity anomaly map (Fig. 6). In order to observe the impact of deep-seated entities, the CBA map was expanded for different continuation distances. The distribution of the regional gravity field at different distances is shown in Fig. 6. At subterranean depths of 0.5, 2.5,

3.5, 5, and 7 km, respectively, gravity effects are detected at the subsequent continuation distances (heights): 1, 5, 7, 10, and 14 km. Shallow-seated bodies are suppressed, while deep-seated bodies are enhanced, as shown in Fig. 6a-d. Low frequency (high wavelength) structures that simulate the impact of deeper and broader Earth structures remain after high frequency structures are filtered out by upward continuation (*Jacobsen, 1987*). The complete Bouguer map at ground level (0 km) in (Fig. 5c) clearly shows the influence of shallow plate sources on deep-seated entities.

On the other hand, when the complete Bouguer map is extended up to 5 km, the elimination of short-wavelength abnormalities and the enhancement of deep-seated entities become visible (Table 2). Four unusual trends are discernible: (i) Gravity responses from deep-seated entities are relatively low on the flanks of the Sokoto Group (Dange and Gamba). (ii) Low gravity responses are observed in the rift margins and floor following the

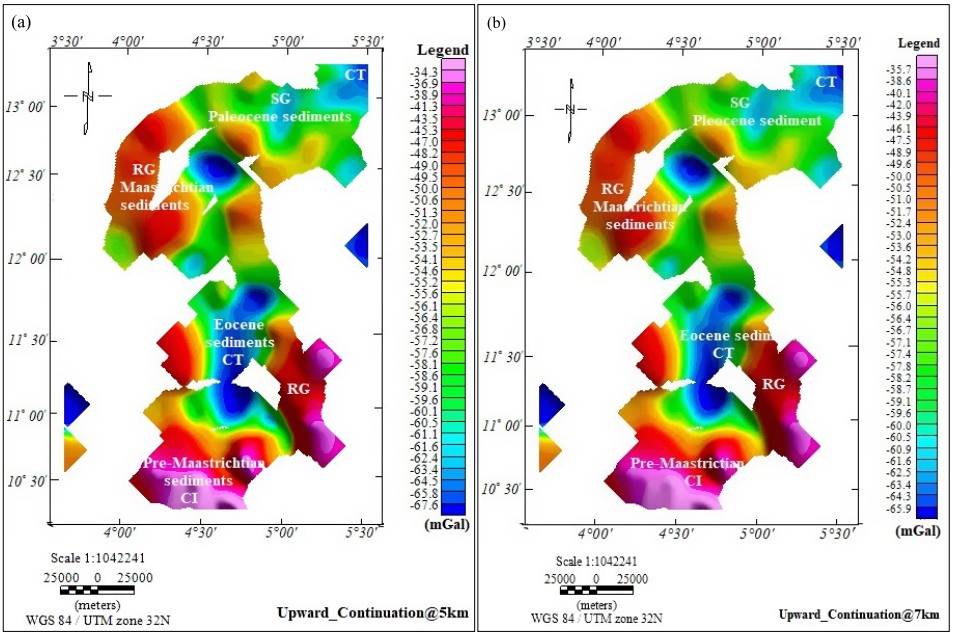

Fig. 6. Regional field map determined by upward continuation at the specific distance: 1 km (a), 5 km (b), 10 km (c), and 14 km (d). Labels: SWP = southwestern plateau, CT = Continental Terminal Gwandu-Eocene, CI = Continental Intercalair pre-Maastrichtian, SG = Sokoto group Paleocene, RG = Rima group Maastrichtian, respectively.

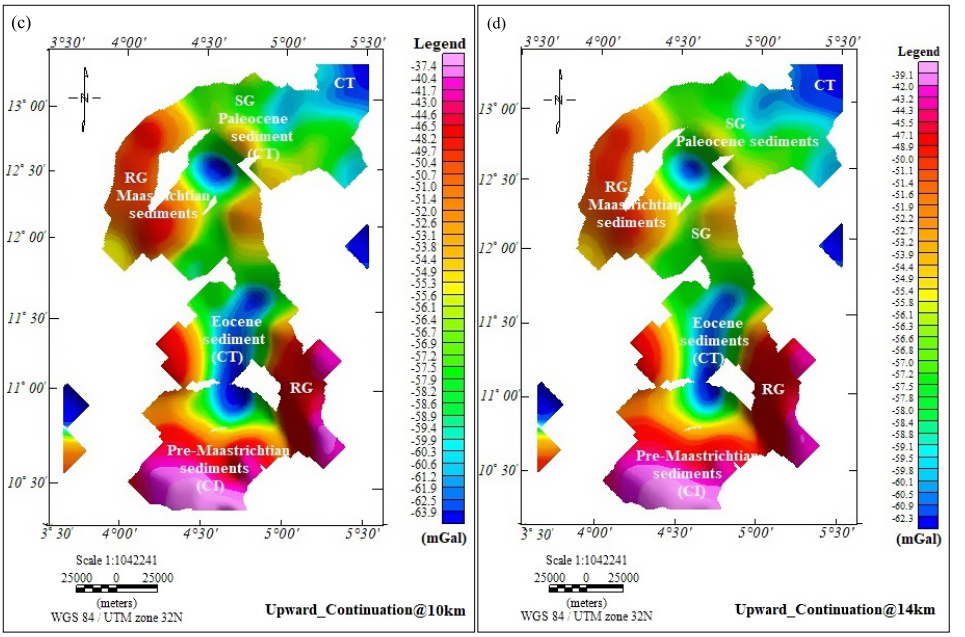

Fig. 6. Continued from the previous page.

southern termination of the West Africa merging area; (iii) intermediate to high gravity responses are observed in the Gundumi-Illo formation and the rift floor; and (iv) a very high gravity field response is observed toward the north following the southern terminus of the Basement complex.

The suppression of shallow-seated entities intensifies these gravity anomaly zones at 5 km, 7 km, and 10 km upward continuation (Figs. 6a-d). With a northward gravity increment along the axis of the profiles, the regional Bouguer anomaly map (Figs. 6a-d) shows the broad regional gravity trend of the Sokoto inland basin. At lesser upward continuation heights, the influence of border faults and structural highs is noticeable as the predominant NE–SW prominent characteristics. A significant increase in the local gravity anomaly is seen northwest of the Rima group (Figs. 6a-d). The Sokoto and Rima groups' respective regions are more developed than the western region, according to previous claims supported by this anomalous signal (*Umego et al., 1992, 1995; Nwanko and Shehu, 2015*).

Table 2. Stratigraphic correlation with faults, after *Obaje et al. (2013)*. Labels: CT – Continental Terminal, CI – Continental Intercalair, SG – Sokoto Group, RG – Rima Group.

Fault influence Zone/Structural interpretation	**Gravity signature**	**Stratigraphic Unit**	**Hydrocarbon Implication**
NW to SE residual anomaly flanks/ Uplifted fault block	Sharp gradients discontinuities +9.2 mGal (High)	RG (Maastrichtian)	Possible faulted traps; sealing structures
Intersecting CT & CI zones (High density intrusion & sedimentary trough)	Low anomalies depressed zones +16.2 mGal (High) & residual lows −14.2 to 2.6 mGal	CI (pre-Maastrichtian) & CT (Eocene)	Migration pathways through fractures
Positive anomalies near SG/Thick sediment	Elevated residual zones −2.7 mGal (Low)	SG (Paleocene)	Potential uplift/ fault-supported reservoir

4.1.4. The residual gravity anomaly map

The residual gravity anomaly map (Fig. 7) reveals a consistent NW–SE alignment of both positive and negative anomalies across the Sokoto Basin. These anomaly trends coincide spatially with key stratigraphic units: Continental Terminal (CT), Continental Intercalair (CI), Sokoto Group (SG), and Rima Group (RG) suggesting underlying structural influences. High-gradient zones within the residual anomalous zone probably coincide with some faults, with lateral offsets estimated between 10 and 12 km (Fig. 7, Tables 1 & 2). The deep gradients are observed RG and SG boundaries, suggesting some uplifted fault blocks or crustal compartmentalisation. Subdued anomaly zones within CI formations exhibit subtle troughs and low-density corridors, potentially marking migration pathways for hydrocarbons from deeper formations (Fig. 7, Tables 1 & 2).

The strong NW–SE residual gravity signature supports the presence of deep-seated basement faults probably related to the basin's structural evolution. Residual lows within CI zones align with mapped seepage sites and may represent fault-controlled vertical migration corridors (Fig. 7, Tables 1 & 2). The N–S trending faults intersecting major NE–SE structures act as secondary conduits, with residual anomalies along these features showing subdued gradients that may reflect sedimentary infill or fault sealing.

Residual highs flanking the SG and RG units likely indicate uplifted fault blocks forming structural traps. These blocks may create cap-rock architecture critical for hydrocarbon entrapment, especially where they are juxtaposed against impermeable units (*Kogbe, 1979; Obaje et al., 2013*). The structural features derived from gravity anomalies correspond well with mapped stratigraphic units, allowing for positive correlation and alignment of geophysical data and lithological information. This alignment reinforces the role of basement tectonics in shaping petroleum system architecture across the Sokoto Basin.

4.1.5. Geological features and anomaly amplitudes

Several geological structures, such as the Rima group (RG), Sokoto group (SG), Continental intercalaire (CI), and Continental terminal (CT), are delineated by the residual anomalies. These characteristics are found close to

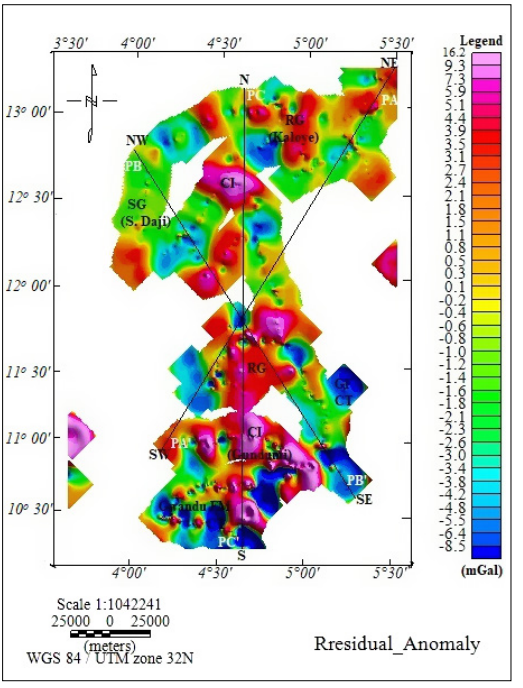

Fig. 7. Residual anomaly map Labels: CT = Continental Terminal Gwandu–Eocene; CI = Continental Intercalair of pre-Maastrichtian sediments; SG = Sokoto group Paleocene sediments; RG = Rima group Maastrichtian sediments, respectively.

the Argungu-Gwandu formation, Kaloye, the Isah-Sabon-Birni structures, Sokoto-Dogon-daji, and the Gundumi/Illo formation.

With amplitude of +9.2 mGal, the anomaly above the Rima group (RG) in Sokoto-Dogon-daji shows a high gravity. The anomaly over the Sokoto group (SG), on the other hand, has a low gravity with amplitude of −2.7 mGal (Fig. 7, Table 2). Gravity amplitudes of the anomalies over the Gwandu Continental Terminal (CT), close to the Argungu-Gulma communities, range from −14.2 mGal to +2.6 mGal. The Gundumi and Illo formations have a positive anomaly with amplitude of +16.2 mGal, which corresponds to a continental intercalaire (CI) anomaly. Prominent NE–SW trends in the southern zone exhibit clear structural alignments that correlate with known pre-existing basement faults, likely the ones reactivated during the early stages of basin rifting (Fig. 7, *Kogbe, 1979; Obaje et al., 2013*). These fault systems appear to control uplifted basement blocks and may have facilitated the emplacement of intrusive bodies, expressed in the gravity data as localised highs. Residual gravity anomalies, together with EBTHG results, indicate that these are deep-seated, high-gradient structures, interpreted as basin-segmenting transfer faults. Such faults exert a strong influence on the spatial distribution of sedimentary facies and play a critical role in the development of structural traps and hydrocarbon migration pathways (*Kogbe, 1979, 1981; Obaje et al., 2013*). The N–S trending structures occur as secondary lineaments intersecting the dominant NE–SW and NW–SE fault systems. These are interpreted as younger strike-slip or transcurrent faults, possibly accommodating stress redistribution during later tectonic phases (Fig. 7; Table 2). Depending on their geometry and kinematics, these faults may act either as secondary migration conduits or as sealing barriers for hydrocarbons.

4.1.6. Density contrast and geological implications

The high gravity in the vicinity of the Gundumi and Illo formation indicates a good density variance with the basement or adjacent rocks. Thickened sediments over the Paleocene Sokoto group or the Gwandu formations are consistent with the area's reported gravity lows (Fig. 7, Table 2). A strong link may be seen between the geology map and the residual anomaly map.

Based on the Bouguer map, the most prominent gravity high Continental intercalaire (CI) anomaly is found in the Gundumi and Illo formations,

which are situated outside the Pre-Maastrichtian sediment zone. There might be a high-density intrusion in the foundation underneath, which would explain this gravity high. The presence of high-density intrusive rocks, like red molten ironstone, cannot be completely ruled out, but substantial sedimentary overburden may be the cause of a low relative gravity (*Kogbe, 1979; 1981*).

4.2. Application of enhancements filters and depth analysis to gravity data

To gain a deeper understanding of the gravity data, we employed various techniques and filters, including power spectrum analysis, 2D and 3D models, enhanced balanced total horizontal gradient, and directional filtering. These methods enabled us to estimate depths and detect edges. The residual anomaly of the gravitational sources is presented in Fig. 7.

4.2.1. Enhance balanced total horizontal gradient

The EBTHG technique provides a more detailed representation of subsurface features compared to horizontal derivative gravity, as evident in Figure 8. This map simultaneously enhances short-and long-wavelength anomalies, offering a clearer image of lithological and structural discontinuities. The colour scale legend helps identify the edges (borders) of source bodies, distinguishing between the source body, edge, and outside source bodies. The EBTHG technique also sharpens the peaks of gravity anomalies and widens weak anomaly signals, making it useful for locating deep sources (*Pham, 2023; Salem et al., 2011*). Strong density differences are shown by anomalies with high gradient values, while minima in the EBTHG map (Fig. 8) describe the area near the Continental Terminal of the Gwandu's Eocene deposits. The viewing of both shallow and deep-seated subsurface entities is enhanced by this filtered map. In Figure 8, the striking faults that indicate the direction of boundary faults—NE-SW, E-W, and NW-SE—are prominently displayed at their respective sites.

4.2.2. Directionally filtered gravity map

A Fourier-based method was used to transform the Bouguer and residual gravity anomalies, producing directionally filtered data that highlighted particular features. Following filtering, the data was inversely Fourier converted

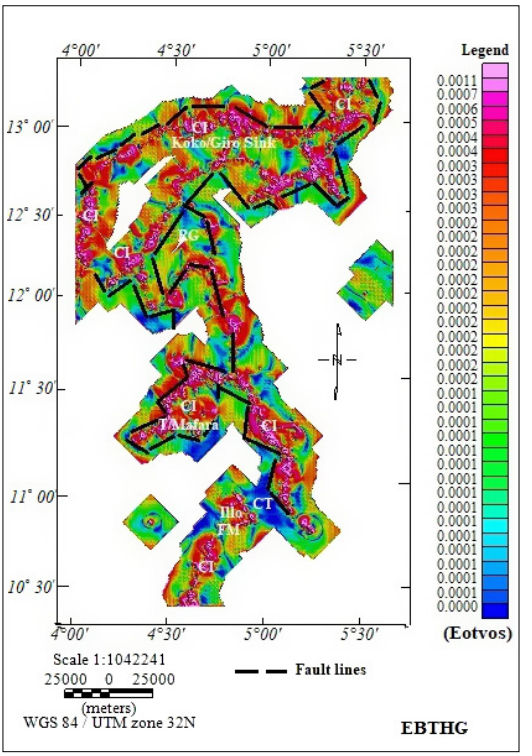

Fig. 8. Enhance balanced total horizontal gradient map over the Study area. Labels: CT = Continental Terminal of Gwandu Formation, CI = Continental Intercalair of Gundumi/Illo Formation, SG = Paleocene sediments of Sokoto groups, RG = Maastrichtian sediments of Rima group.

into the space domain. Figure 9 shows the result of using a 45° directional filter aimed at the northeast, which includes the Rima groups who noted that linear features on topographic maps can show the positions of vertical movements, tilting, or horizontal displacements, which are frequently interpreted as faults or lineaments. We colour-coded the directionally filtered maps to highlight areas where patterns were disrupted (Fig. 9). The fault structures are successfully enhanced in the final map, which makes the underlying geological characteristics easier to see. Enhanced edge detection filtering further refines these interpretations by suppressing noise and clarifying contact zones, validating the correlation between residual gravity signatures and subsurface fault dynamics.

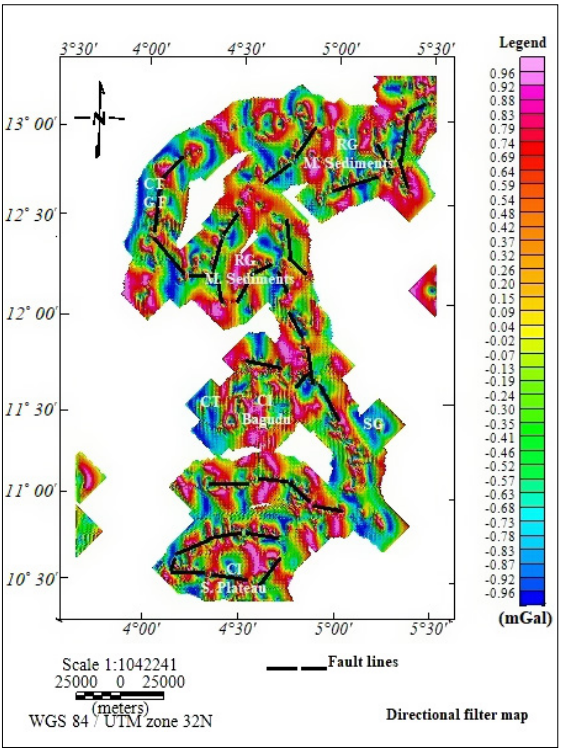

Fig. 9. Directionally filter gravity map of the Study area. Labels: CT = Continental Terminal of Gwandu Formation, CI = Continental Intercalaire of Gundumi/Illo Formation, SG = Paleocene sediments of Sokoto groups, RG = Maastrichtian sediments of Rima group.

4.2.3. Depth estimation and source characterisation

As illustrated in Figure 10, the logarithm of spectral energy plotted against wavenumber represents the computed average power spectrum derived from gravity anomaly data. Using a piece-wise least-squares linear curve fitting method, linear segments were fitted to the power spectrum to estimate the depth to the top of gravity sources (density interfaces). The spectral energy was categorised into low, intermediate, and high-frequency bands, representing deep, intermediate, and shallow sources, respectively. The dominance of low-frequency components indicates that a significant portion of the anomaly arises from deep-seated sources. The estimated depth to the

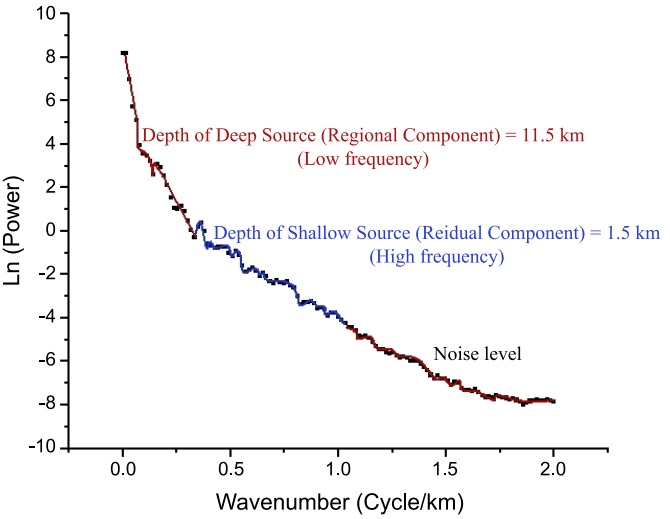

Fig. 10. Average power spectrum curve with their depth estimation.

deepest sources is approximately 11.5 km, aligning with values observed in comparable tectonic settings within West Africa. *Nwankwo (2015)* reported similar deep anomalies within the Iullemmeden Basin, reaching depths of 10–12 km. *Obaje et al. (2013)* also noted deep-seated magnetic sources in the Sokoto Basin, confirming the reliability of the current estimates. The shallow source depth of approximately 1.5 km corresponds to the thickness of younger sedimentary covers, particularly within the Gwandu Formation. These values are consistent with shallow source depths of 0.7 to 2.0 km reported by *Kogbe (1981)*. Table 3 provides a summary of spectral depth estimates across different structural blocks. Deep source depths range between 3.04 km and 8.91 km, while shallow plate sources vary between 1.16 km and 4.59 km. These estimates correlate well with lithostratigraphic data from well logs and boreholes (*Kogbe, 1979;* Table 1), thereby validating the spectral approach. For example, the depth of 4.54 km (Block 1) aligns with the base of the Illo/Gundumi formations where intrusive bodies are known to occur, as discussed by *Adamu et al. (2021)*. The third segment of the power spectrum accurately defines the data noise threshold, thereby enhancing the robustness of the interpreted depth estimates. This tripartite division into noise, residual, and regional components is consistent with gravity interpretation methodologies described by *Telford et al. (1990)*.

Table 3. Depth estimates for the deep (regional), shallow (residual), and noise components of the subsurface anomalous source, with their uncertainties of each of the blocks.

Blocks	DDpt	UErr	DSha	UErr	LApp	LInf
1	8.91	0.36	4.54	0.02	Intrusive bodies layers	at the bottom of Ilo/Gundumi
2	6.40	0.21	4.06	0.05	Lacustrine shale layers	at Dukamaje
3	4.12	0.10	2.41	0.08	Quaternary layers	at Gwandu
4	3.04	0.09	1.77	0.06	Lacustrine shale layers	at Taloka
5	4.90	0.31	2.87	0.07	over the layers of gravel	at the bottom of Illo
6	5.02	0.27	4.59	0.16	Shale strata with variegation	Dukamaje/Dange
7	3.99	0.10	1.16	0.06	Intrusive bodies layers	at the bottom of Illo
8	3.77	0.33	1.53	0.02	Lacustrine shale layers	at Dukamaje
9	4.25	0.06	1.74	0.04	Top of gravel layer	at Taloka

Legend: DDpt = Depth to Regional (Components) (Deep, km); DSha = Depth to Residual (Components) (Shallow, km); UErr = Uncertainty Error (± m); LApp = Lithostratigraphic approximation from Table 1; LInf = Litho-structural Information.

4.2.4. Werner depth gravity analysis

The depth and location of gravity sources along the rift axis were further assessed using the Werner deconvolution technique. Table 4 presents the results of this automated inversion, identifying vertical contacts and dyke-like structures. The estimated depths from the Werner method (ranging from 3.2 to 4.5 km) correspond well with the intermediate depths derived from spectral analysis. Structural alignments inferred from the Werner solutions show strong conformity with fault patterns observed in residual gravity maps.

4.3. Interpretation of the residual anomalies

Residual gravity anomalies were analysed to outline the subsurface structural configuration. Profile A–A' indicates gravity lows and highs that correlate with the Gulma and Duku-Tarasa escarpments. These are attributed

Table 4. Investigation of Werner deconvolution anomalous depth profiles using statistics.

Trend	No	Par	Dmin	Dmax	Dmean	SD	Remarks
N to S	1	Z_Contacts Z_Dykes	−4210.46 −4507.12	−0.25 −0.23	−125.39 −189.20	130.25 110.06	Estimates vertical sources
NE to SW	2	Z_Contacts Z_Dykes	−3245.51 −3450.04	−0.18 −0.14	−110.28 −122.90	143.23 107.12	//
NW to SE	2	Z_Contacts Z_Dykes	−3756.98 −3865.90	−1.34 −1.13	−140.32 −137.08	167.21 189.09	//
E to W	4	Z_Contacts Z_Dykes	−3989.54 4032.54	−0.21 −0.18	165.89 −173.32	156.98 142.76	//
Total	**9**						

Legend: No = Numbers; Par = Parameter; Dmin = Minimum depth (m); Dmax = Maximum depth (m); Dmean = Mean depth; SD = Standard deviation (m).

to mafic intrusions with a density contrast of approximately 0.30 g/cm^3, and these match the values reported for similar intrusive bodies in the region by *Kogbe (1979)*. Profiles B–B′ and C–C′ traverse the Illo and Rima formations and display gravity signatures corresponding to basement undulations, consistent with previous models from the Iullemmeden Basin (*Obaje et al., 2013*). The main goal of interpreting quantitative gravity data is to identify a subsurface structure that reflects the gravity field that is observed. The deeper the underlying structure, the greater the anomaly's size. This method mainly uses geologic data, highlighting the importance of having a sufficient understanding of the local geology. The Eocene-aged sediments in the research area are part of the Gwandu Formation and have an average density of roughly 2.35 g/cm^3 (Tables 4 & 5). Paleocene and Maastrichtian deposits (Kalambaina, Dange, Gamba, Wurno, Dukamaje, and Taloka formations) make up the underlying strata. Their average densities are roughly 2.40 and 2.55 gcm^{-3}, respectively. As stated by *Kogbe (1979, 1981)*, these deposits reach a depth of about 270 metres. Along with continental deposits (the Illo and Gundumi formations) at roughly 700 m, which have an average density of 2.64 gcm^{-3}, there is a lower Cretaceous or Pre-Maastrichtian deposit below this depth (*Kogbe, 1979*, Tables 4 & 5). The value 2.35 gcm^{-3} is the estimated mean density of the sediments covering the basement rocks. Although the interpretation method employed in this work is vulnerable to model ambiguities, it is beneficial because most ambiguities are kept within reasonable ranges by geological and geophysical constraints. Ac-

cording to the profile constructed on the residual anomaly, the substantial Duku-Tarasa and Gulma magnetic anomaly is located exactly where the aeromagnetic data shows a strong magnetic low in the northern region of Argungu and Birnin Kebbi (*Adamu et al., 2021*). This confirms that the gravity data's location and magnitude of this anomaly are accurate.

Table 5. Density contrasts vs. observed lithologies used for the purpose of analysis (*Kogbe, 1979; Telford et al., 1990*).

Observed lithologies	**Density range (gcm^{-3})**	**Average density (gcm^{-3})**
Overburden soil	1.24 – 2.4	1.92
Sandstone	1.61 – 2.72	2.35
Sand	1.7 – 2.3	2.0
Gravel	1.7 – 2.4	2.0
Clay	1.63 – 2.6	2.21
Shale	1.77 – 3.20	2.40
Limestone	1.93 – 2.90	2.55
Basalt	2.70 – 3.30	2.99
Acidic igneous rocks	2.30 – 3.17	2.61
Metamorphic	2.4 – 3.1	2.74
Basic igneous rocks	2.09 – 3.17	2.79
Mafic intrusions	2.50 – 2.81	2.64
Schist	2.39 – 2.90	2.64

4.4. Gravity models

The residual gravity anomaly was used to build two-dimensional gravity models. Profiles A–A′, C–C′, and B–B′ (Fig. 7) that run along the rift axis were the profiles along which measured anomaly values were obtained. In order to create 2D models, these profiles were specifically selected to intersect at the Gwandu continental terminal (CT).

4.4.1. 2D gravity model along and across the selected profiles

In Figure 11, Profile A–A′ crosses the Gwandu formation and extends north-south. This profile runs north to south across the anomalies of the Gwandu formations. A gravity low is shown at around 4.5 km from the southern end, while two gravity highs are visible at about 2.0 and 6.0 kilometres. A density contrast of -0.20 gcm^{-3} in the sedimentary strata led to the introduction

of two escarpment structures, Gulma and Duku-Tarasa (Fig. 11, Table 4), to explain the low and intermediate gravity values. A causative body at the profile's southwest end has a density contrast of 0.30 gcm^{-3} (Table 4). With a dip angle of almost 35 degrees on either flank, this body is roughly 3.0 km long and extends to 6.0 km. The "Gore" in Fokku, which is an intrusive entity inside the Gundumi formation, is responsible for the high gravity along the profile.

Profile B–B′, shown in Figure 12, passes through the Rima group and Illo formation in a NE–SW direction. This profile's basement intrusions were described, with the southern part of the profile dominated by the Gwamba scarp in the Illo formation. According to Figs. 2 and 12, the profile shows two gravity highs at 4 and 10 km, respectively, and a gravity low at 3 km from the southwest end. The eastern part of the Rima group has a gravity low, which can be explained by a density differential of 2.0 gcm^{-3} in the ore deposit (Table 4).

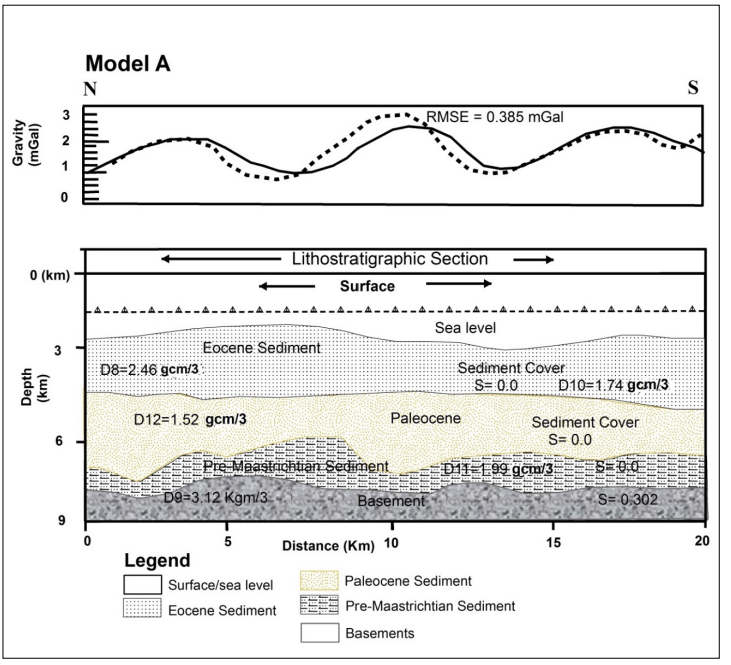

Fig. 11. Two-dimensional gravity model over the profile A–A′. In this case, g_{calc} (dashed line) stands for the calculated gravity and g_{obs} (solid line) for the observed gravity.

By crossing the Rima group (Wurno-Rabah and the Sokoto-Bodinga-Tambuwal trenches), Profile C–C′ (Fig. 13) moves from the NW to SE of the Sokoto group to the NE to SW of the Gundumi formation. This region is regarded as a potential hydrocarbon exploration site (*Obaje et al., 2013*). When the model is seen, the lateral and vertical discontinuities of geological formations and structures such as intrusive bodies and buried weak zones and faults can be clearly seen.

4.4.2. 3D model of shallow structural features of Sokoto Basin

The 3D geophysical model (Fig. 14) presents an integrated image of upper lithospheric architecture. Basement depths vary between 2.5 and 9.0 km along selected profiles. The deepest parts coincide with areas of low gravity and thick sedimentary cover. These interpretations are consistent with *Kogbe's (1981)* structural division of the Sokoto Basin. The model illustrates

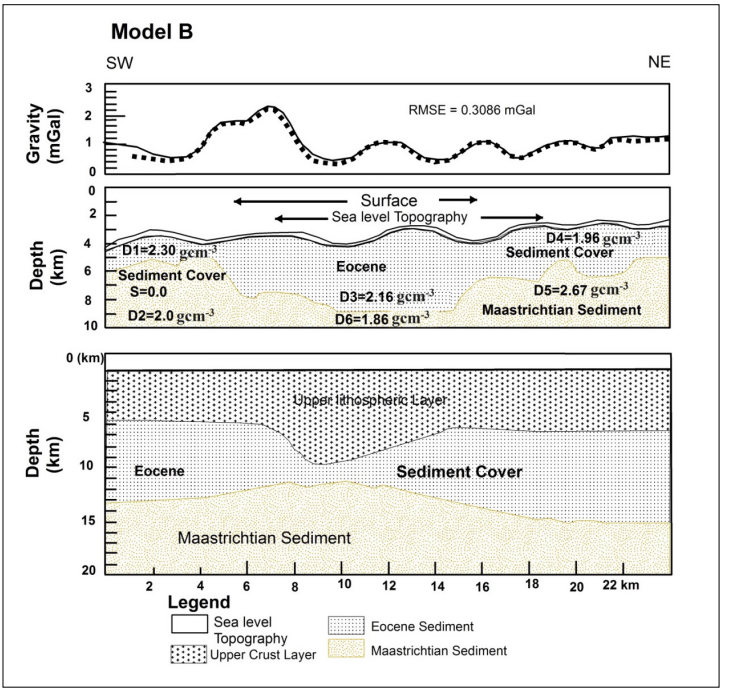

Fig. 12. 2D gravity model along the profile B–B′ crossing the Sokoto basin. Here, g_{obs} (solid) represents the observed gravity and g_{calc} (dashed) represents the calculated gravity.

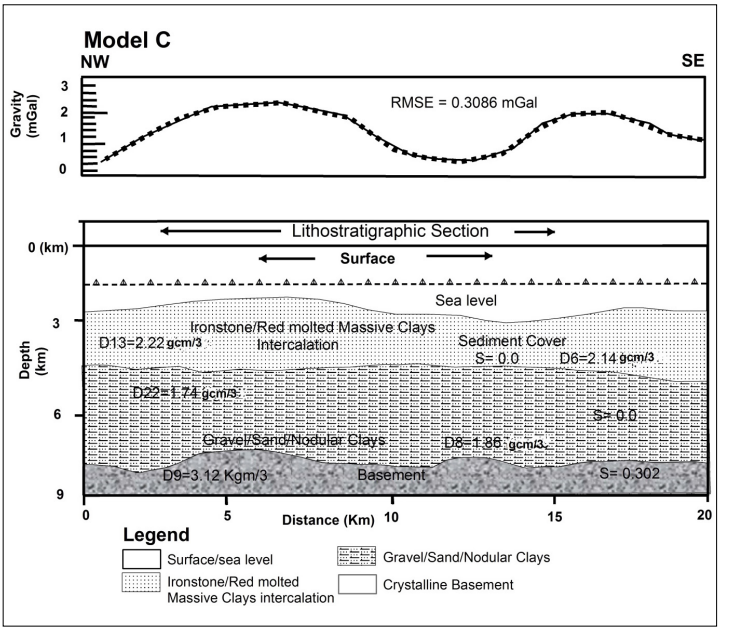

Fig. 13. 2D gravity model across the profile C–C′ crossing the Sokoto basin. Here, g_{obs} (solid) represents the observed gravity and g_{calc} (dashed) represents the calculated gravity.

ridges, trenches, and intrusive features, affirming the complex tectonic evolution of the region.

4.5. Depth extent, density contrast and lithological correlation

Density contrasts derived from gravity modelling are consistent with lithological units mapped in the study area. For instance, the Gwandu Formation exhibits an average density of 2.35 gcm^{-3}, while intrusive bodies are denser, averaging 2.64 gcm^{-3}. These values correspond closely with the ranges reported by *Telford et al. (1990)* and support the stratigraphic correlations established from well-log data (Table 6). An approximate depth extension of 9 km was found in both profiles. The intrusion's density contrast is 2.3 gcm^{-3}, and its depth extension is 3 km. The depths to the top of the basement vary between roughly 9.0 and 2.5 kilometres along and across the three profiles. To comprehend the structure beneath the Sokoto basin, subsurface modelling was carried out, which showed that comparable density interfaces varied in depth. It is in line with the findings of *Kogbe (1979,*

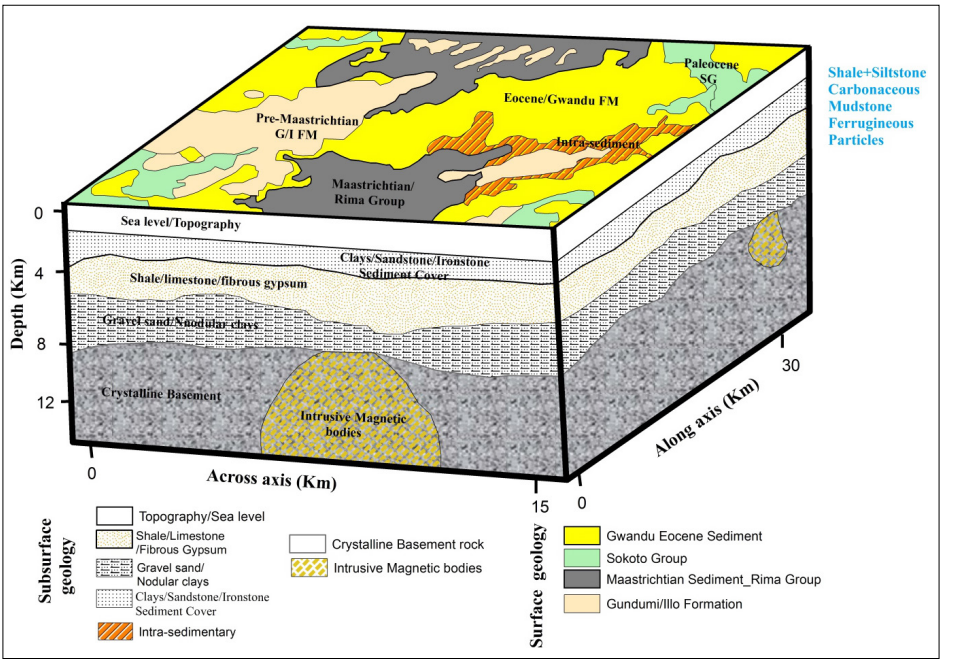

Fig. 14. 3D architecture of the upper lithospheric structures beneath the Sokoto Basin.

1981), who proposed that the northwest structural high of the Gwandu formation divides the northern and central portions of the Sokoto basin. The geological map shows that the Quaternary rift sediment ($\rho = 2.38$ gcm^{-3}, Table 4) is the top density layer, covering the majority of the rift floor (Fig. 2). This second layer includes the Sokoto group ($\rho = 2.14$ gcm^{-3}, Table 4), the Eocene Gwandu formations, the Gamba shale and claystone ($\rho = 2.49$ gcm^{-3}, $\rho = 2.42$ gcm^{-3}, Table 4), and the Kalambaina formation, which unconformably covers the Wurno-Rima group ($\rho = 2.24$ gcm^{-3}) (*Kogbe, 1979*). According to several authors, Maastrichtian sediments are present in the northern section of the Iullemmeden basin, despite the fact that the thickness of these formations is not well constrained (*Kogbe, 1979, 1981; Obaje et al., 2013*).

4.6. Structural framework and basement depth

The fault planes and depressions of the shallow plate sources are revealed by the inclusion of ferruginous rocks from the Sokoto and Gwandu groups.

Table 6. Comparative summary of findings.

Parameter	**Present study**	**Ko79, Ko81, Ob13**	**Nw15**	**Interpretation**
Deep source depth	∼11.5 km	∼5 to 12 km	∼11.5 to 28 km	Matches regional basement estimates
Shallow source depth	∼1.5 km	∼0.7 to 2.0 km	∼1.2 to 1.8 km	Reflects younger sedimentary thickness
Density contrast	2.21 to 2.64 gcm^{-3}	2.2 to 2.7 gcm^{-3}	2.3 to 2.6 gcm^{-3}	Consistent with regional lithologies
Intrusive bodies	Confirmed	Confirmed	Confirmed	Inferred from gravity anomalies

Legend: Ko79 = *Kogbe (1979)*; Ko81 = *Kogbe (1981)*; Ob13 = *Obaje et al. (2013)*; Nw15 = *Nwankwo (2015)*.

The shallow structural characteristics of the Sokoto basin were formed by the movement of intra-sedimentary units to deep subsurface plate sources. Because of underlying anomalies, the zones in the Sokoto Basin have various structural frameworks due to discontinuity or lack thereof. The power spectrum analysis for deep sources is compatible with the 3D model's basement depth, which indicates a deep basement (11.5 km). The findings of power spectrum analysis and the 3D block exhibit a strong correlation (Table 2).

5. Conclusions

This study presents a comprehensive investigation of the gravity data over the southwestern Sokoto Basin, utilizing digital filtering techniques such as enhanced balanced total horizontal gradient, directional filtering, spectrum analysis, and 2D Werner depth analysis. The key findings of this study are:

(i) Gravity data confirm significant anomalies at Duku-Tarasa and Gulma, with low negative anomalies and localised highs caused by high-density materials with average densities of approximately 2.75 gcm^{-3} probably indicating the presence of ferruginous rocks (a probable reservoir?). This is a future exploration target. The escarpment is centred roughly 2-km depth anomalies.

(ii) The dip estimates of the primary scarp-producing anomalies vary from 20° to 48°, with lateral extents of 3 and 6 km, respectively. Inward-

dipping (convergent) walls are observed in certain places within Gwandu formation; there is a 40-m thick layer of carbonaceous shale as reported by *Kogbe (1979)* and recently by the Kebbi State Ministry of Mines and Steel Development.

(iii) Source depths tend to deepen toward the south, as indicated by 2D spectral depth analysis of gravity data and their joint 2D forward modelling.

(iv) The 3D gravity model agrees with surface geological features and depth measurement techniques, providing two depth estimates of 1.80 and 2.93 km, which closely correspond to the locations of two density interfaces.

(v) Upper crust gravity modelling reveals intrusions at depths of 10 to 20 km and 5 to 10 km, respectively, in the up-dip sections of the Taloka and Gundumi-Illo Formations.

The study also highlights the impacts of faults on hydrocarbon systems in the southwestern Sokoto Basin: Quaternary faults and fractures in the Eocene sediment at the Gwandu Continental Terminal play a crucial role in the local hydrocarbon system, influencing sediment cover and potentially enabling vertical migration through the Eocene seals. The faults and fractures may provide pathways for hydrocarbon accumulation and migration: highlighting the importance of understanding fault geometry for future hydrocarbon exploration.

Acknowledgements. The authors wish to express their sincere gratitude to the Federal University Birnin Kebbi, Nigeria, for its financial support for this project through the 2023/2024 TETFund research grant. Additionally, the authors gratefully acknowledge the Nigerian National Petroleum Cooperation for facilitating the acquisition of Gravity data used in this study, particularly to one of the authors (AA). The authors also appreciate all the reviewers, including editors, for their constructive comments which eventually contributed to improving our manuscript.

Funding. The authors declare financial support was received for the research and authorship of this article. This work was in part financially assisted by Federal University Birnin Kebbi, through Tertiary Education Trust Fund (TETfund) Nigeria local grant intervention.

Conflict of interest. On behalf of all authors, I declare that there is no potential conflict of interest.

References

Abraham E., Abdufarraj M., Ikeazota I., Afuwai C., Obande E., 2025: Crustal thickness and lithospheric thermal state beneath the West African sub-region from modelling gravity and magnetic anomalies. Geosci. J., **29**, 5, 742–758, doi: 10.1007/s12303-025-00047-y.

Adamu A., Likkason O. K., Maigari A. S., Ali S., Agada E. M., 2021: Subsurface investigation of geological structures from magnetic method in parts of Kangiwa Gwandu Formation northwestern, Nigeria. In: Baker H., Miller R. (Eds.): Proc. Sixth International Conference on Engineering Geophysics, virtual, 25–28 October 2021. SEG Global Meeting Abstracts, pp. 336–341, doi: 10.1190/iceg2021-085.1.

Agarwal B. N. P., Sivaji Ch., 1992: Separation of regional and residual anomalies by least-squares orthogonal polynomial and relaxation techniques: a performance evaluation. Geophys. Prospect., **40**, 2, 143–151, doi: 10.1111/j.1365-2478.1992.tb00368.x.

Ai H., Alvandi A., Ghanati R., Pham L. T., Saad S. A., Nasui D., Eldosouky A. M., 2023: Modified non-local means: A novel denoising approach to process gravity field data. Open Geosci., **15**, 1, 20220551, doi: 10.1515/geo-2022-0551.

Ali M., Halidu H., Mijinyawa A., 2016: Stratigraphic Review of the Cretaceous Tertiary Deposits of the Iullemmeden Basin in Niger and Nigeria. Asian J. Appl. Sci., **4**, 2, 540–547.

Bamberger R. H., Smith M. J. T., 1992: A filter bank for the directional decomposition of images: theory and design. IEEE Transactions on Signal Processing, **40, 4,** 882–893, doi: 10.1109/78.127960.

Chen Z., Mou L., Meng X., 2016: The horizontal boundary and top depth estimates of buried source using gravity data and their applications. J. Appl. Geophys., **124**, 62–72, doi: 10.1016/j.jappgeo.2015.11.003.

Chen H., 2019: Gravity, magnetic, and electromagnetic surveys' applications and challenges. In: Sun J. (Ed.): International Workshop on Gravity, Electrical & Magnetic Methods and Their Applications, Xi'an, China. Society of Exploration Geophysics. SEG Global Meeting Abstracts, pp. 13–16., doi: 10.1190/GEM2019-004.1.

Cooper G. R. J., 1997: GravMap and PFproc: Software for filtering geophysical map data. Comput. Geosci., **23**, 1, 91–101, doi: 10.1016/S0098-3004(96)00064-7.

Dobrin M. B., 1976: Introduction to Geophysical Prospecting (3rd ed.). McGraw-Hill Book Co., New York, 630 p.

Fairhead J. D., 1986: Geophysical controls on sedimentation within the African Rift Systems. In: Frostick L. E., Renaut R. W., Reid I., Tiercelin J. J. (Eds.): Sedimentation in the African Rifts. Geol. Soc. Spec. Publ., **25,** 19–27, doi: 10.1144/GSL.SP.1986.025.01.03.

Fedi M., Mastro S., 2018: Bounded-region wavelet spectrum: A new tool for depth estimation of gravity and magnetic data. In: Alumbaugh D., Bevc D. (Eds.): SEG International Exposition and 88th Annual Meeting, Anaheim, California, USA, October 2018. Paper Number: SEG-2018-2998315, SEG Technical Program Expanded Abstracts, 1425–1429, doi: 10.1190/segam2018-2998315.1.

Hartman R. R., Teskey D. J., Friedberg J. L., 1971: A system for the rapid digital aeromagnetic interpretation. Geophysics, **36**, 5, 891–918, doi: 10.1190/1.1440223.

Hinze W. J., von Frese R. R. B., Saad A. H., 2013: Gravity and Magnetic Exploration: Principles, Practices, and Applications. Cambridge University Press, New York, 525 p., doi: 10.1017/CBO9780511843129.

Hu J. V., Rabiner L. R., 1972: Design techniques for two-dimensional digital filters. IEEE Trans. Audio Electroacoust., **20**, 4, 249–257, doi: 10.1109/TAU.1972.1162399.

Jacobsen B. H., 1987: A case for upward continuation as a standard separation filter for potential-field maps. Geophysics, **52**, 8, 1138–1148, doi: 10.1190/1.1442378.

Kebede H., Alemu A., Fisseha S., 2020: Upward continuation and polynomial trend analysis as a gravity data decomposition, case study at Ziway-Shala basin, central Main Ethiopian rift. Heliyon, **6**, 1, e03292, doi: 10.1016/j.heliyon.2020.e03292.

Kogbe C. A., 1979: Geology of the Southeastern (Sokoto) Sector of the Iullemmeden Basin. Bull. Geol. Dep. Ahmadu Bello Univ. Zaria Nigeria, **2**, 1, 42–64.

Kogbe C. A., 1981: Cretaceous and Tertiary of the Iullemmeden Basin in Nigeria (West Africa). Cretac. Res., **2**, 2, 129–186, doi: 10.1016/0195-6671(81)90007-0.

Kowalik W. S., Glenn W. E., 1987: Image processing of aeromagnetic data and integration with Landsat images for improved structural interpretation. Geophysics, **52**, 7, 875–884, doi: 10.1190/1.1442358.

Ku C. C., Sharp J. A., 1983: Werner deconvolution for automated magnetic interpretation and its refinement using Marquardt's inverse modelling. Geophysics, **48**, 6, 754–774, doi: 10.1190/1.1441505.

Likkason O. K., 2011: Spectral Analysis of Geophysical Data. In: Chen D. (Ed.): Advances in Data, Methods, Models and Their Applications in Geoscience. Intech-Open, pp. 27–52, doi: 10.5772/28070.

Likkason O. K., Singh G. P., Samaila N. K., 2013: A Study of the Middle Benue Trough (Nigeria) Based on Geological Application and Analyses of Spectra of Aeromagnetic Data. Energy Sources, Part A: Recovery, Utilization, and Environmental Effects, **35**, 8, 706–716, doi: 10.1080/15567036.2010.514588.

Maithya J., Fujimitsu Y., 2018: Analysis and Interpretation of Gravity Data to delineate structural features in Eburru Geothermal Field of Kenya. In: Watanabe T. (Ed.): Proc. 13th SEGJ International Symposium, Tokyo, Japan, 12-14 November 2018. SEG Global Meeting Abstracts, pp. 216–219, doi: 10.1190/SEGJ2018-058.1.

Mekkawi M. M., 2012: Application of Magnetic Method in Mineral Exploration: Iron-Ore Deposit, South Zagros Suture Zone. J. Egypt. Geophys. Soc., **10**, 1, 117–124, doi: 10.21608/jegs.2012.384986.

Mekkawi M. M., ElEmam A. E., Taha A. I., Al Deep M. A., Araffa S. A. S., Massoud U. S., Abbas A. M., 2021: Integrated geophysical approach in exploration of iron ore deposits in the North-eastern Aswan-Egypt: a case study. Arab. J. Geosci., **14**, 721, doi: 10.1007/s12517-021-06964-0.

Menke W., 1989: Geophysical Data Analysis: Discrete Inverse Theory (1st ed.). Academic Press.

Mickus K., Tadesse K., Keller G. R., Oluma B., 2007: Gravity analysis of the main Ethiopian rift. J. Afr. Earth Sci., **48,** 2-3, 59–69, doi: 10.1016/j.jafrearsci.2007.02.008.

Mishra D. C., Naidu P. S., 1974: Two-dimensional power spectral analysis of aeromagnetic fields. Geophys. Prospect., **22**, 2, 345–353, doi: 10.1111/j.1365-2478.1974.tb00090.x.

Mohamed A., Al Deep M., 2021: Depth to the bottom of the magnetic layer, crustal thickness, and heat flow in Africa: Inferences from gravity and magnetic data. J. Afr. Earth Sci., **179**, 104204, doi: 10.1016/j.jafrearsci.2021.104204.

Moussa S. A. W., Abdel Nabi S. H., Araffa S. A., Mansour S. A., Al Deep M. A. I., 2020: Geophysical exploration of titanomagnetite ore deposits by geomagnetic and geoelectric methods. SN Appl. Sci., **2**, 3, 444, doi: 10.1007/s42452-020-2206-5.

Naidu P. S., 1968: Spectrum of the potential field due to randomly distributed sources. Geophysics, **33**, 2, 337–345, doi: 10.1190/1.1439933.

Naidu P. S., Mathew M. P., 1998: Digital analysis of aeromagnetic maps: Detection of a fault. J. Appl. Geophys., **38**, 3, 169–179, doi: 10.1016/S0926-9851(97)00024-4.

Nwakwo L. I., 2015: Estimation of depths to the bottom of magnetic sources and ensuing geothermal parameters from aeromagnetic data of Upper Sokoto Basin, Nigeria. Geothermics, **54**, 76–81, doi: 10.1016/j.geothermics.2014.12.001.

Nwankwo L. I., Shehu A. T., 2015: Evaluation of Curie-point depths, geothermal gradients and near-surface heat flow from high-resolution aeromagnetic (HRAM) data of the entire Sokoto Basin, Nigeria, Nigeria. J. Volcanol. Geotherm. Res., **305,** 45–55, doi: 10.1016/j.jvolgeores.2015.09.017.

Obaje N. G., 2009: Introduction. In: Geology and mineral resources of Nigeria. Lecture Notes in Earth Sciences, **120**, Springer/book series, Berlin Heidelberg, pp. 1–9, doi: 10.1007/978-3-540-92685-6_1.

Obaje N. G., Aduku M., Yusuf I., 2013: The Sokoto Basin of northwestern Nigeria: A preliminary assessment of hydrocarbon prospectivity. Pet. Technol. Dev. J., **3**, 2, 66–80.

Pham L. T., 2023: A novel approach for enhancing potential field: application to aeromagnetic data of the Tuangiao, Vietnam. Eur. Phys. J. Plus, **138**, 12, 1134, doi: 10.1140/epjp/s13360-023-04760-1.

Pham L. T., Prasad K. N. D., 2023: Analysis of gravity data for extracting structural features of the northern region of the Central Indian Ridge. Vietnam J. Earth Sci., **45**, 2, 147–163, doi: 10.15625/2615-9783/18206.

Pham L. T., Abdelrahman K., Nguyen D. V., Gomez-Ortiz D., Long N. N., Luu L. D., DO T. D., Vo Q. T., Nguyen T.-H. T., Nguyen H.-D. T., Eldosouky A. M., 2024: Enhancement of the balance total horizontal derivative of gravivity data using the power law approach. Geocarto Int., **39**, 1, 2335251, doi: 10.1080/10106049.2024.2335251.

Reid A. B., Allsop J. M., Granser H., Millet A. J., Somerton I. W., 1990: Magnetic interpretation in three dimensions using Euler deconvolution. Geophysics, **55**, 1, 80–91, doi: 10.1190/1.1442774.

Reid A. B., Thurston J. B., 2014: The structural index in gravity and magnetic interpretation: Errors, uses, and abuses. Geophysics, **79**, 4, J61–J66, doi: 10.1190/geo2013-0235.1.

Salem A., Williams S., Fairhead J. D., Ravat D., Smith R., 2007: Tilt-depth method: A simple depth estimation method using first-order magnetic derivatives. Lead. Edge, **26**, 12, 1502–1505, doi: 10.1190/1.2821934.

Salem S. M., Arafa S. A., Ramadan T. M., El-Gammal E. A., 2011: Exploration of copper deposits in Wadi-ElRegeita area, Southern Sinai, Egypt, with contribution of remote sensing and geophysical data. Arab. J. Geosci., **6**, 2, 321–335, doi: 10.1007/s12517-011-0346-z.

Spector A., Grant F. S., 1970: Statistical models for interpreting aeromagnetic data. Geophysics, **35**, 2, 293–302, doi: 10.1190/1.1440092.

Talwani M., Worzel J. L., Landisman M., 1959: Rapid gravity computations for two-dimensional bodies with application to the Mendocino submarine fracture zone. J. Geophys. Res., **64**, 1, 49–59, doi: 10.1029/JZ064i001p00049.

Tarlowski C., McEwin A. J., Reeves C. V., Barton C. E., 1996: Dewarping the composite anomaly map of Australia using control traverses and base stations. Geophysics, **61**, 3, 696–705, doi: 10.1190/1.1443997.

Telford W. M., Geldart L. P., Sheriff R. E., 1990: Applied Geophysics. Cambridge, Cambridge University Press.

Thorarinsson F., Magnusson S. G., Bjornsson A., 1988: Directional spectral analysis and filtering of geophysical maps. Geophysics, **53**, 12, 1587–1591, doi: 10.1190/1.1442440.

Treitel S., Shanks J. L., Fraiser C. W., 1967: Some aspects of the fan filtering. Geophysics, **32,** 789–800, doi: 10.1190/1.1439889.D. C.

Turner D. C., 1983: Upper Proterozoic schist belts in the Nigerian sector of the Pan-African Province of West Africa. Precambrian Res., **21**, 1-2, 55–79, doi: 10.1016/0301-9268(83)90005-0.

Umego M. N., Ojo S. B., Dyrelius D., Ajakaiye D. E., 1992: Magnetic anomaly map of the Sokoto basin, Northwestern Nigeria: Compilation and preliminary interpretation. J. Min. Geol., **28**, 2, 309–315.

Umego M. N., Ojo S. B., Ajakaiye D. E., 1995: A magnetic depth to basement analysis in the Sokoto basin, North Western Nigeria. J. Min. Geol., **31**, 161–167.

Werner S., 1953: Interpretation of magnetic anomalies at sheet-like bodies. Sveriges Geologiska Undersökning (SGU) Årsbok (Swedish Geological Survey Yearbook), Ser. C, no. 508, **43**, 6.